ACCSCIENCE PUBLISHING

Microbes & Immunity

ORIGINAL RESEARCH ARTICLE

Cellular and molecular characteristics of low-grade central nervous system tumors revealing modulations in Ki-67/propidium iodide, MMP2, VEGFR2, and CD11b/Iba1: Analyses of post-operative samples

Krishnendu Ghosh[1,2,3], Pritha Bhattacharjee[2], and Anirban Ghosh[1,4*]

[1]Immunobiology Laboratory, Department of Zoology, Panihati Mahavidyalaya (West Bengal State University), Sodepur, West Bengal, India

[2]Environmental Epigenomics Laboratory, Department of Environmental Science, University of Calcutta, Kolkata, West Bengal, India

[3]Department of Pathology, Carver College of Medicine, University of Iowa, Iowa City, Iowa, United States of America

[4]Cell Development and Immunobiology Laboratory, Department of Zoology, School of Sciences, Netaji Subhas Open University, Kolkata, West Bengal, India

***Corresponding author:**
Anirban Ghosh
(anirbanghosh@wbnsou.ac.in; aghosh06@gmail.com)

Citation: Ghosh K, Bhattacharjee P, Ghosh A. Cellular and molecular characteristics of low-grade central nervous system tumors revealing modulations in Ki-67/propidium iodide, MMP2, VEGFR2, and CD11b/Iba1: Analyses of post-operative samples. *Microbes & Immunity*. 2025;2(3):130-144. doi: 10.36922/MI025190040

Received: May 8, 2025

Revised: June 5, 2025

Accepted: June 6, 2025

Published online: July 16, 2025

Abstract

The World Health Organization's 2016 and 2021 classifications of central nervous system (CNS) tumors emphasize the integration of histopathological and molecular profiling for improved prognostic and therapeutic precision. Understanding the molecular hallmarks of low-grade CNS tumors is essential for enabling precision therapies and minimizing off-target effects while preventing malignant transformation. This study investigated key oncogenic features in surgically resected low-grade CNS tumors of varying cellular lineages and anatomical locations, alongside associated clinical metadata. Tumors were histologically classified and analyzed for molecular markers using immunohistochemistry, immunofluorescence microscopy, and flow cytometry. Assessed hallmarks included proliferation (Ki-67, propidium iodide index), invasiveness (matrix metalloproteinase [MMP]-2), neovascularization (vascular endothelial growth factor receptor 2 [VEGFR2], epigenetic modulation (DNA methyltransferase 1 [DNMT1], and immune microenvironment (Cluster of Differentiation 11b [CD11b], Iba1, silver-gold macrophage staining). Statistical analyses included *t*-tests, one-way ANOVA, and Kruskal–Wallis tests ($p<0.05$). In diffuse astrocytoma and myxopapillary ependymoma, a proliferation–invasion dichotomy was observed, with lower-proliferative ependymomas exhibiting higher MMP-2 expression. Astrocytomas exhibited elevated DNMT1 expression, indicative of increased epigenetic alterations. Immune profiling revealed tumor-specific differences: $CD11b^+$ macrophages were more prominent in meningiomas, while $Iba1^+$ microglia were enriched in astrocytomas, reflecting distinct immune microenvironments. Despite their low-grade classification, these tumors demonstrated hallmark cancer characteristics, variably expressed across astrocytoma, ependymoma, and meningioma. The combined assessment of Ki-67, MMP-2, VEGFR2, DNMT1, CD11b, and Iba1 provides a prognostically informative and therapeutically exploitable profile. These findings support the integration of molecular profiling into risk stratification and adjunctive

treatment strategies to improve prognosis and reduce malignant progression in low-grade CNS tumors.

Keywords: Low-grade tumor; Astrocytoma; Ependymoma; Meningioma; Proliferation; Neo-vascularization; Invasion; Immune microenvironment

1. Introduction

Primary central nervous system (CNS) tumors represent a broad category of malignancies with an incidence rate of approximately 5 – 10 cases/100,000 individuals in India. Although they account for only 2 – 2.5% of all malignancy cases, they are associated with significant morbidity and mortality.[1] A foundational cross-sectional study analyzing 39,509 cancer patient records from multiple hospitals and institutions in Kolkata, India, reported that 2.4% of all CNS malignancies were primary CNS tumors, among which 60% were gliomas, followed by meningioma, medulloblastomas, primitive neuroectodermal tumors, and others.[2] Another prospective epidemiological study reported that 59.6% of all astrocytic tumors were high-grade astrocytomas, which account for 38.7% of all astrocytic neoplasms in the study population.[3] More recently, a clinico-epidemiological study from Gauhati Medical College, Assam, India, reported that 30% of all diagnosed brain tumors were glioblastoma multiforme, followed by 15% each for grade II and grade III astrocytomas.[4]

CNS tumors are found to be more common in males and frequently occur in individuals aged 40 – 60 years. Over two decades of surveillance have shown an increasing trend in CNS tumor incidence in the Indian population, with overall poor due to the relatively high prevalence of gliomas despite recent therapeutic advancements.[1,2,5] Similarly, data from the Central Brain Tumor Registry of the United States indicate that malignant brain tumors are higher in males, with a modest increase in overall survival in recent years; however, outcomes in elderly glioblastoma multiforme patients have demonstrated only marginal improvement.[6]

These findings suggest that the middle-aged Indian population is more susceptible to glial-origin CNS tumors than others, with prognosis heavily dependent on early diagnosis and treatment modules. Since radiological assessments are often limited by diagnostic variability, and other non-invasive diagnostic methods remain elusive,[7] molecular profiling has emerged as a critical tool for identifying detailed tumor phenotypes – essential for accurate prognostication and personalized therapeutic interventions.[8] Accordingly, molecular profiling is now prominently featured in the revised editions of the World Health Organization (WHO) Classification of Tumors of the CNS, particularly the 4th and 5th editions. In 2016, the WHO introduced integrated molecular and histological criteria for CNS tumor classification, which were further expanded in the 2021 edition with greater emphasis on molecular characterization.[9,10] The importance of these changes is increasingly evident as tumor samples reveal molecular features that are either type- or grade-specific, or in some cases, shared across subtypes.

The molecular characterization of CNS tumors has advanced significantly with the identification of key biomarkers. Ki-67 is a reliable marker of cell proliferation, with expression levels markedly elevated in high-grade tumors.[11] Matrix metalloproteinase (MMP)-2 shows moderate expression in low-grade gliomas, reflecting limited invasiveness and an intact blood–brain barrier (BBB), but becomes significantly upregulated in high-grade tumors, facilitating extracellular matrix degradation and invasive growth.[12] Vascular endothelial growth factor receptor 2 (VEGFR2) is minimally expressed in low-grade tumors, indicating relatively stable vascular architecture and limited angiogenesis, but is highly expressed in advanced CNS neoplasms, where it is related to pathological angiogenesis and microvascular proliferation.[13] Immune markers, such as Cluster of Differentiation 11b (CD11b), a leukocyte/macrophage marker, and Iba1, a CNS macrophage/microglia marker, play important roles in shaping the tumor immune microenvironment. In high-grade CNS tumors, expression levels of CD11b and Iba1 increase substantially, reflecting an altered immune landscape with greater invasion potential.[14] Moreover, tumor-associated macrophages in high-grade tumors tend to polarize toward the CD206^{+} M2 phenotype, which promotes pro-tumorigenic activity – a feature largely absent in low-grade tumors.[15] DNA methyltransferase 1 (DNMT1) also displays grade-specific expression, remaining relatively low in low-grade tumors, consistent with stable DNA methylation patterns. In contrast, DNMT1 is significantly upregulated in high-grade tumors, contributing to widespread CpG island hypermethylation and silencing of tumor suppressor gene.[16] Given the strong associations between these molecular markers, tumor phenotypes,

and their prognostic and therapeutic relevance, the present study incorporated Ki-67, MMP-2, VEGFR2, CD11b, Iba1, and DNMT1 for characterization.

In the present work, we analyzed histopathology and molecular hallmarks of three types of low-grade CNS tumors: spinal myxopapillary ependymoma, fibroblastic meningioma, and diffuse astrocytoma. Low-grade CNS tumors pose considerable clinical challenges due to their unpredictable progression and the lack of reliable prognostic biomarkers. Present diagnostic modalities often fail to predict which tumors will undergo malignant transformation, when this transition might occur, and how aggressively the disease may evolve. Consequently, therapeutic strategies remain suboptimal, adversely affecting patient outcomes.

Moreover, the tumor microenvironment and cellular dynamics that drive progression from indolent to aggressive phenotypes remain poorly characterized, representing a critical knowledge gap in neuro-oncological research. Accordingly, this study aimed to: (i) conduct a comparative analysis of key molecular ontogenic profiles between glial and non-glial low-grade CNS tumors to reveal physiological differences; (ii) determine whether these molecular hallmarks represent viable, subtype-specific therapeutic targets; and (iii) explore whether these molecular characterizations could inform the development of targeted therapies with improved efficacy and reduced off-target toxicity.

Although limited by a small sample size, this study offers a unique contribution to understanding the molecular landscape of low-grade CNS tumors. It may aid in diagnosis, risk stratification, and therapeutic decision-making. Ultimately, this approach seeks to bridge fundamental tumor biology with clinical application, offering potential pathways for early intervention strategies that could prevent malignant transformation and enable more effective targeted therapies.

2. Methodology

2.1. Tumor samples, histology, and metadata

Post-operative CNS tumor tissues were collected from the Bangur Institute of Neurosciences, Institute of Post Graduate Medical Education and Research (IPGME&R), Kolkata, India. Samples were preserved in (i) 10% buffered formalin (CDH, India) for histopathological and immunohistochemical analysis, (ii) 4% paraformaldehyde (MERCK, India) for immunofluorescence studies, and (iii) serum-free Dulbecco's Modified Eagle Medium (DMEM) (Gibco Invitrogen, United States of America [USA]) for live cell isolation and flow cytometry.

Formalin-fixed tissues were processed with embedding and sectioned at 10 μm using a microtome (WESWOX, India). Sections were mounted on glass slides, deparaffinized through alcoholic dehydration, stained with hematoxylin and eosin (Merck, India), and observed under a bright field microscope (TS100F Eclipse, Nikon Corp., Japan). Images were captured using a CCD camera (DS-Fi2-U3, Nikon Corp., Japan).

Tumor type and grade were determined by a collaborating pathologist based on histological features, following the 2016 WHO classification of CNS tumors. A total of 10 low-grade tumor samples were obtained: three spinal myxopapillary ependymomas, four fibroblastic meningiomas, and three diffuse astrocytomas. These tumors are frequently underdiagnosed and are typically identified only after progression to higher-grade lesions, which limits the number of available samples. Additional clinical data included magnetic resonance imaging (MRI) scans with T1- and T2-weighted contrast-enhanced imaging and magnetic resonance spectroscopy (MRS), focusing on N-acetylaspartate (NAA) peaks and choline/creatine ratios. The use of post-operative human tumor tissues adhered to ethical guidelines approved by the Institutional Ethical Committee, IPGME&R, Kolkata (vide Memo No. Inst/IEC/553, dated January 15, 2014).

2.2. Silver/gold (SG) staining of paraffin-embedded tissue

Silver staining and gold toning were performed on 10 μm paraffin-embedded tissue sections. After fixation and deparaffinization, sections were stained using freshly prepared ammoniacal silver carbonate (CDH, India), followed by rinsing in 10% formalin. Subsequently, the sections were toned in gold chloride (Loba Chemie, India) and then fixed in sodium thiosulfate (MERCK, India). Microscopic analysis was carried out using the same imaging system as described in Section 2.1. Images were acquired using the NIS Element-BR software (Nikon Corp., Japan) to identify electron-dense macrophages and microglia.

2.3. Tissue preparation for immunofluorescence microscopy

Tissues were fixed in 4% paraformaldehyde (MERCK, India), washed, and stored in phosphate-buffered saline (PBS; CDH, India) at 4°C. Specimens were sectioned at a thickness of 10 μm, and separate immunofluorescence staining protocols were applied using the following antibodies: glial fibrillary acidic protein (GFAP)-Alexa Fluor 488-conjugated monoclonal antibody (mAb) (Cat. No. 561449, BD Pharmingen, USA), CD11b-FITC mAb (Cat. No. 101205, BioLegend, USA), and Iba1 mAb

(Cat. No. ab5076, Abcam, USA) with a PE-conjugated, anti-mouse, human cross-reactive polyclonal secondary antibody (Cat. No. ab98742, Abcam, USA). In addition, VEGFR2 mAb (Cat. No. sc-6251, Santacruz, USA) was used with a TRITC-conjugated secondary antibody (Cat No. ab6786, Abcam, USA), and MMP-2 mAb (Cat. No. NB200-114, Novus Biologicals, USA) was paired with a FITC-conjugated secondary antibody (Cat. No. ab6785, Abcam, USA).

Non-conjugated primary antibodies were used at a 1:500 dilution, while conjugated primary and secondary antibodies were used at a 1:1000 dilution. All antibodies were diluted in 5% fetal bovine serum (GIBCO, USA) in PBS. Incubations were performed in a dark, humid chamber. A blocking-permeabilizing buffer was prepared using 5% FBS in PBS containing 0.25% Tween-20 (MERCK, India). Fluorescence imaging was conducted using the previously mentioned microscope equipped with EpiFL-B2A and EpiFL-G2A filters (for Alexa Fluor 488/FITC and PE/TRITC, respectively; Nikon Corp., Japan). Images were captured and processed using the previously mentioned CCD camera and imaging software. Mean fluorescence intensity (MFI) was quantified, plotted, and subjected to statistical analysis.

2.4. Immunohistochemistry with counterstaining

Tissue sections were incubated at 54°C overnight, then hydrated and washed with PBS. Blocking was performed using 3% bovine serum albumin (LOBA, India), followed by overnight incubation with non-conjugated Ki-67 mAb (Cat. No. sc-23900, Santacruz, USA) and DNMT1 mAb (Cat. No. sc-271729, Santacruz, USA) at a 1:200 dilution. The slides were then washed and incubated with a horseradish peroxidase-conjugated secondary antibody (Cat. No. ab97030; Abcam, USA) at 1:500 in ×1 PBS. Development was achieved using 3,3-diaminobenzidine (SRL, India) in buffered H_2O_2 (1M TRIS, pH 7.4) supplemented with 0.5% cupric sulfate, in the dark for 20 minutes. Sections were counterstained with hematoxylin (Merck, India), followed by graded alcohol dehydration, air drying, and mounting. Slides were examined using the same microscopic system. For Ki-67 quantification, the number of Ki-67-positive cells were counted and divided by the total number of cells within each microscopical field to calculate the proliferative index. Data were tabulated, graphed, and statistically analyzed.

2.5. Cell isolation, culture, and immunophenotyping

Freshly excised tumor samples were aseptically collected in serum-free DMEM at 4 – 6°C and mechanically minced. Samples were enzymatically dissociated using 0.25% trypsin-ethylenediaminetetraacetic acid (EDTA) (Sigma Aldrich, USA). FBS (MP Biomedicals, USA) was added to neutralize trypsin, and the suspension was filtered through a 70 µm nylon mesh (HiMedia, India). The filtrate was centrifuged and resuspended in DMEM. Cells were counted and seeded in 60 mm culture dishes (Greiner, Germany) at a density of 2×10^6 cells in DMEM supplemented with 10% FBS and 2% antibiotic-antimycotic solution (HiMedia, India). Cultures were maintained in a humidified incubator at 37°C with 5% CO_2 (New Brunswick, Eppendorf, United Kingdom) for 2 days. Following incubation, cells were detached using Accutase (Sigma-Aldrich, USA), washed, and fixed with 4% paraformaldehyde. Cell pellets were treated with permeabilizing blocking buffer (5% FBS in PBS with 0.5% Tween-20) and then washed. Immunostaining was performed using MMP-2 mAb (Cat. No. NB200-114, Novus Biologicals, USA) at a 1:500 dilution and a PE-conjugated secondary antibody (Cat. No. ab97024, Abcam, USA) at a 1:700 dilution. After staining, pellets were washed and analyzed using a BD-FACS Verse flow cytometer with Verse-Suit 1.0 software (BD Biosciences, USA).

2.6. Cell cycle analysis from paraffin-fixed tissue

Cell cycle ploidy analysis was performed on paraffin-embedded tumor tissues as previously described.[10,17] Briefly, 90 µm ribbons were sectioned from paraffinized tissue blocks and treated with xylene (MERCK, India). The resulting pellet was collected through centrifugation, subjected to descending alcohol gradation, and washed repeatedly with PBS. Antigen retrieval was performed using citrate buffer, followed by incubation. Samples were then digested with 0.25% trypsin-EDTA, washed in PBS, and filtered through a 70 µm nylon mesh. The filtrate was centrifuged and resuspended in PBS. RNaseA (1 mg/mL; Invitrogen, USA) was added and incubated at 37°C. Propidium iodide (PI; 0.5 mg/mL; Life Technologies, USA) was then added, followed by incubation. Samples were analyzed using the BD Accuri C5 flow cytometer (BD Biosciences, USA). The cumulative percentage of cells in the S+G2M phases was used as an indicator of proliferation and was subsequently graphed and analyzed statistically.

2.7. Statistical analysis

All experiments were performed in triplicate for each sample. Depending on the data distribution and experimental design, non-parametric tests and/or *t*-tests were applied. Statistical significance was assessed using the Kruskal–Wallis test and nested one-way ANOVA, performed with GraphPad Prism® 10 for Windows 64-bit, version 10.4.2 (633). A $p \leq 0.05$ was considered statistically significant. Additional statistical tests were employed where appropriate. Full statistical details, including significance levels, are provided in the figure legends.

3. Results

3.1. Histopathological findings, MRI metadata, and evaluation of glial/non-glial nature

Histopathological analysis at ×100 and ×400 magnifications revealed distinct architectural features for each tumor type. Ependymoma exhibited lobulated, island-like patterns with hyalinized fibrovascular cores and characteristic perivascular pseudorosettes (Figures 1B and 1C). Meningioma demonstrated classic "whorling" formations resulting from interlacing fascicles of fibroblastic origin (Figure 1F and 1G). In diffuse fibrillary astrocytoma, we noted increased glial cell density and a prominent fibrillary network (Figure 1J and 1K). Among the astrocytoma specimens, nuclear atypia and pleomorphism – hallmarks of malignancy – were most pronounced. Vascular proliferation was most extensive in astrocytoma, followed by lobular-specific vascular islands in ependymoma and moderate, sprouting vasculature in meningioma.

Dystrophic microcalcifications were most abundant within the lobules of ependymoma, moderately dispersed in astrocytoma, and sparse in meningioma. Each tumor type exhibited a distinct histoarchitectural profile. The progressive increase in nuclear atypia and vascular proliferation from meningioma to ependymoma to astrocytoma suggests an escalating degree of biological aggressiveness, even within low-grade classifications.

MRI of myxopapillary spinal ependymoma (Figure 1A) revealed a heterogeneous lesion extending from L1 to L5, with a loss of normal lumbar curvature. The lesion appeared iso- to hyperintense on T2-weighted images. MRS demonstrated a markedly elevated choline peak and a significantly reduced NAA peak. In meningioma (Figure 1E), imaging revealed a large extra-axial mass in the midline basifrontal region, showing intense post-contrast enhancement. The mass appeared iso- to hypointense on T1 and iso- to mildly hyperintense on T2-weighted sequences,

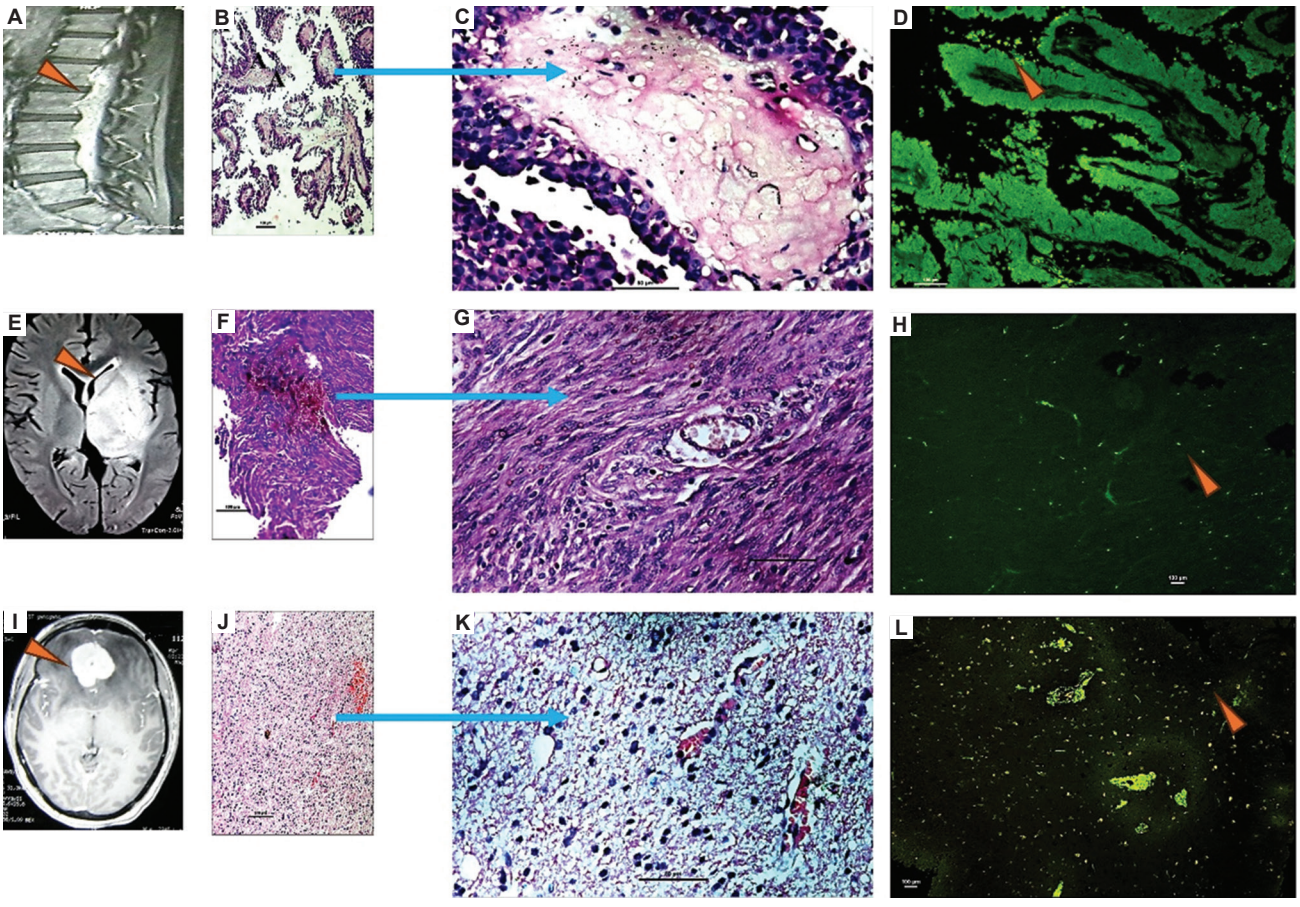

Figure 1. Radiological, histopathological, and immunofluorescence analysis of tumor samples. Low-grade spinal myxopapillary ependymoma: T1- and T2-weighted magnetic resonance (MR) images of (A); Hematoxylin and eosin (H&E)-stained histopathological sections at ×100 (scale bar: 100 μm) and ×400 (scale bar: 50 μm) magnification (B and C); Glial fibrillary acidic protein (GFAP) immunofluorescence (D), with glial cells indicated by orange arrows; Low-grade fibroblastic meningioma: MR images (E); H&E-stained sections at ×100 (scale bar: 100 μm) and ×400 (scale bar: 50 μm) magnification (F and G); GFAP immunofluorescence, with glial cells indicated by orange arrows (H); Low-grade diffuse astrocytoma: MR images (I); H&E-stained sections at ×100 (scale bar: 100 μm) and ×400 (scale bar: 50 μm) magnification (J and K); GFAP immunofluorescence, with glial cells indicated by orange arrows (L).

with mild midline shift and compression effects. MRS indicated increased choline and predominantly reduced NAA levels. Intracranial diffuse astrocytoma (Figure 1I) demonstrated an ill-marginated region of altered signal intensity in the left temporo-parietal region, appearing hypointense on T1 and hyperintense on T2-weighted images. The lesion was associated with a distinct mass effect and midline shift. MRS showed highly elevated choline levels and significantly reduced NAA peaks. Across all tumor types, consistently increased choline and reduced NAA levels reflected altered cellular metabolism characteristic of neoplastic transformation. Among these, astrocytoma displayed the most pronounced metabolic disruption, consistent with its higher malignant potential.

GFAP immunofluorescence revealed extensive astrocytic involvement in low-grade astrocytoma (Figure 1L), with numerous GFAP-positive cells indicating glial hypercellularity. Spinal ependymoma exhibited significantly fewer GFAP-positive cells (Figure 1D), while meningioma demonstrated minimal GFAP expression (Figure 1H), consistent with its origin from GFAP-negative meningio-epithelial cells.

3.2. Immunocytochemistry and immunofluorescence assay corroborates cell-cycle, proliferation, and neo-angiogenesis

Immunohistochemical analysis of Ki-67 expression revealed distinct proliferative profiles among the three tumor types. Astrocytoma demonstrated the highest Ki-67 expression (Figure 2C), whereas ependymoma (Figure 2A) and meningioma (Figure 2B) exhibited comparatively lower expression. Quantitative assessment of Ki-67-positive cell indices yielded mean values of 0.62 ± 0.09 for ependymoma, 1.34 ± 0.36 for meningioma, and 2.1 ± 0.16 for astrocytoma. Statistical analysis confirmed significant differences in proliferative indices across all tumor types, with the most marked disparity observed between ependymoma and astrocytoma (Figure 2D).

Flow cytometric analysis using PI staining corroborated the Ki-67 findings. Cell cycle distribution analysis demonstrated that astrocytoma exhibited the highest percentage of cells in active proliferative phases (S+G2/M: 20.40 ± 2.06%) (Figure 2I and 2J), followed by meningioma (S+G2/M: 12.60 ± 0.70%) (Figure 2G and 2H) and ependymoma (S+G2/M: 8.63 ± 0.51%) (Figure 2E and 2F). Comparative analysis revealed statistically significant differences, confirming that astrocytoma displayed markedly elevated proliferative activity relative to the other two tumor types (Figure 2K).

Given that neoangiogenesis represents a fundamental hallmark of malignancy, we further assessed the angiogenic potential of these tumors through VEGFR2-targeted immunofluorescence using TRITC-conjugated antibodies. Qualitative examination revealed enhanced neovascularization in astrocytoma (Figure 2N) compared to meningioma (Figure 2M) and spinal ependymoma (Figure 2L). Quantitative analysis of MFI values demonstrated statistically significant differences: astrocytoma (59.66 ± 2.55), ependymoma (30.10 ± 2.38), and meningioma (21.35 ± 2.35) (Figure 2O).

These findings collectively indicate a progressive increase in angiogenic activity that correlates with the observed proliferative indices. This suggests a coordinated upregulation of both proliferative and angiogenic signaling pathways in astrocytoma, distinguishing it from other low-grade CNS tumor types.

3.3. MMP-2 expression and invasive potential in low-grade tumor types

Flow cytometric analysis revealed that the MFI of MMP-2-PE was highest in ependymoma (Figure 3A), followed by astrocytoma (Figure 3C), and with the lowest expression observed in meningioma (Figure 3B). To further assess gelatinase-dependent invasiveness, we conducted immunofluorescence using MMP-2-FITC. Ependymoma (Figure 3D) exhibited intense, regionally clustered MMP-2 expression, in contrast to the sparse and scattered signal in meningioma (Figure 3E) and the diffuse moderate expression pattern in astrocytoma (Figure 3F). Quantitative analysis of MFI values showed statistically significant differences in MMP-2 expression across tumor types (Figure 3G). Notably, ependymoma, despite its lower proliferative index, demonstrated the highest MMP-2 expression (62.03 ± 9.50), followed by astrocytoma (40.90 ± 2.04) and meningioma (21.30 ± 2.62).

These findings suggest an inverse relationship between proliferative activity and MMP-2-mediated invasive potential, with ependymomas demonstrating the highest gelatinase-dependent invasiveness despite limited proliferation. This observation highlights ependymomas as a potentially underexplored therapeutic target for MMP-2 inhibitors. Furthermore, profiling MMP-2 expression may serve as a diagnostic tool for personalized treatment strategies for low-grade CNS tumors.

3.4. Immune cell infiltration profiles in the studied low-grade CNS tumors based on silver-gold staining, CD11b, and Iba1 expression

SG histochemical staining was employed to visualize electron-dense mononuclear immune cell populations within the tumor microenvironment, leveraging the differential affinity of metallic ions for cytoplasmic

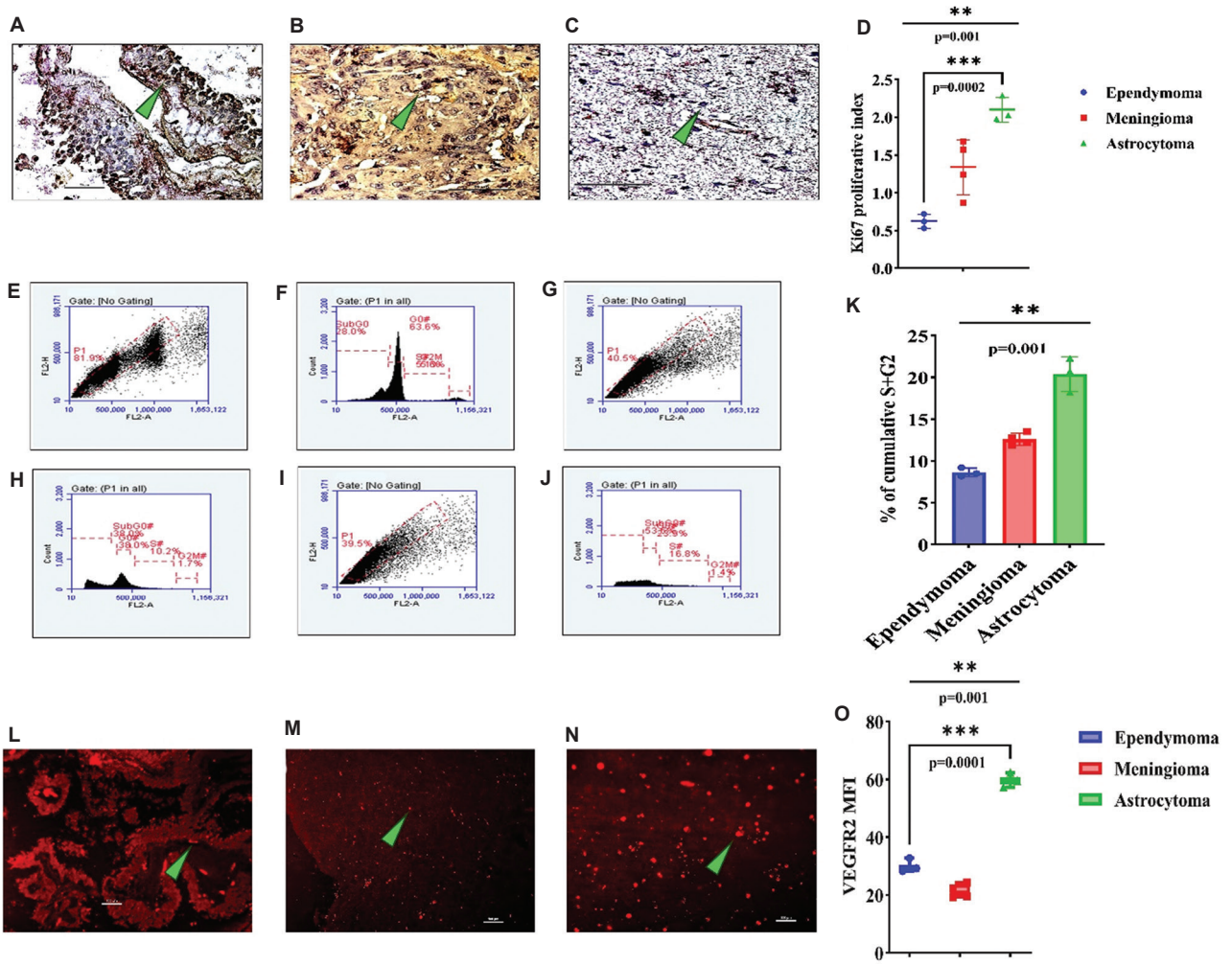

Figure 2. Evaluation of cellular proliferation and associated neoangiogenesis. Ki-67 immunohistochemistry showing proliferative activity (areas marked with green arrows) in: (A) low-grade spinal myxopapillary ependymoma (scale bars: 50 µm; magnification: ×400), (B) low-grade meningioma (scale bars: 50 µm; magnification: ×400), and (C) low-grade astrocytoma (scale bars: 50 µm; magnification: ×400). (D) Quantified Ki-67 proliferative indices plotted and analyzed ***$p \leq 0.001$ ($p=0.0002$; ependymoma versus astrocytoma, unpaired *t*-test); **$p \leq 0.01$ ($p=0.001$; all tumors, Kruskal–Wallis test). Cell cycle analysis using propidium iodide: (E and F) low-grade spinal myxopapillary ependymoma, (G and H) low-grade meningioma, (I and J) low-grade astrocytoma. (K) Cumulative S+G2 phase percentages plotted, with **$p \leq 0.01$ ($p=0.001$; Kruskal–Wallis test). VEGFR2-TRITC IF images (×100, scale bar: 100 µm) (areas marked with green arrows) showing angiogenesis: (L) low-grade spinal myxopapillary ependymoma, (M) low-grade meningioma, (N) low-grade astrocytoma. (O) Box plot of VEGFR2 mean fluorescence intensity data: ***$p \leq 0.001$ ($p=0.0001$; ependymoma vs. astrocytoma, *t*-test); **$p \leq 0.01$ ($p=0.001$; all tumors, Kruskal–Wallis test).
Abbreviations: VEGFR2: Vascular endothelial growth factor receptor 2; TRITC: Tetramethylrhodamine; IF: Immunofluorescence.

components of immune cells. At low magnification (×100), ependymomas (Figure 4A) and astrocytomas (Figure 4E) exhibited comparable levels of immune cell density, whereas meningiomas showed substantially greater infiltration (Figure 4C). High-magnification imaging (×400) revealed the characteristic dark punctate staining of activated macrophages and microglia. Quantitative analysis revealed statistically significant differences in SG-positive cell density across tumor subtypes. Meningiomas exhibited the highest immune cell infiltration (62 ± 3.40; Figure 4D), representing a 1.9-fold increase over ependymomas (32 ± 3.60; Figure 4B) and a 3.4-fold increase over astrocytomas (18 ± 2.5; Figure 4F). *Post hoc* analysis confirmed significant pairwise differences among all tumor groups (Figure 4G), indicating distinct immune microenvironments among CNS tumor subtypes.

Immunofluorescence analysis using CD11b revealed that meningiomas exhibited the highest MFI (27.57 ± 1.23; Figure 4I), followed by ependymomas (9.73 ± 0.60; Figure 4H) and astrocytoma (4.8 ± 0.55; Figure 4J). This

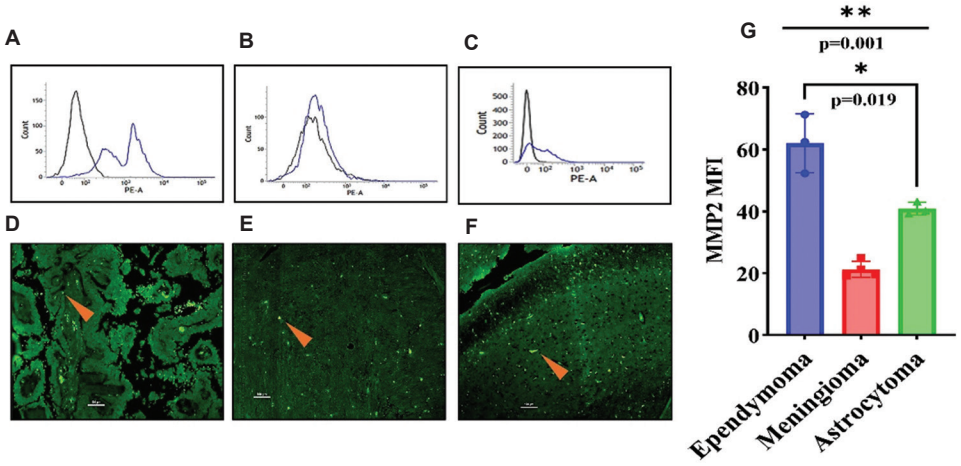

Figure 3. Evaluation of gelatinase-dependent invasiveness. Flow cytometry with PE-conjugated MMP-2 for (A) low-grade spinal myxopapillary ependymoma, (B) low-grade meningioma, (C) low-grade astrocytoma. MMP-2-FITC immunofluorescence images (×100, scale bar: 100 µm) (MMP-2 positive regions marked with orange arrows): (D) low-grade spinal myxopapillary ependymoma, (E) low-grade meningioma, (F) low-grade astrocytoma. (G) Mean fluorescence intensity data plotted: *$p \leq 0.05$ ($p=0.019$; ependymoma vs. astrocytoma, *t*-test); **$p \leq 0.01$ ($p=0.001$; all tumors, Kruskal–Wallis test).
Abbreviations: MMP-2: Matrix metalloproteinase 2; FITC: Fluorescein isothiocyanate.

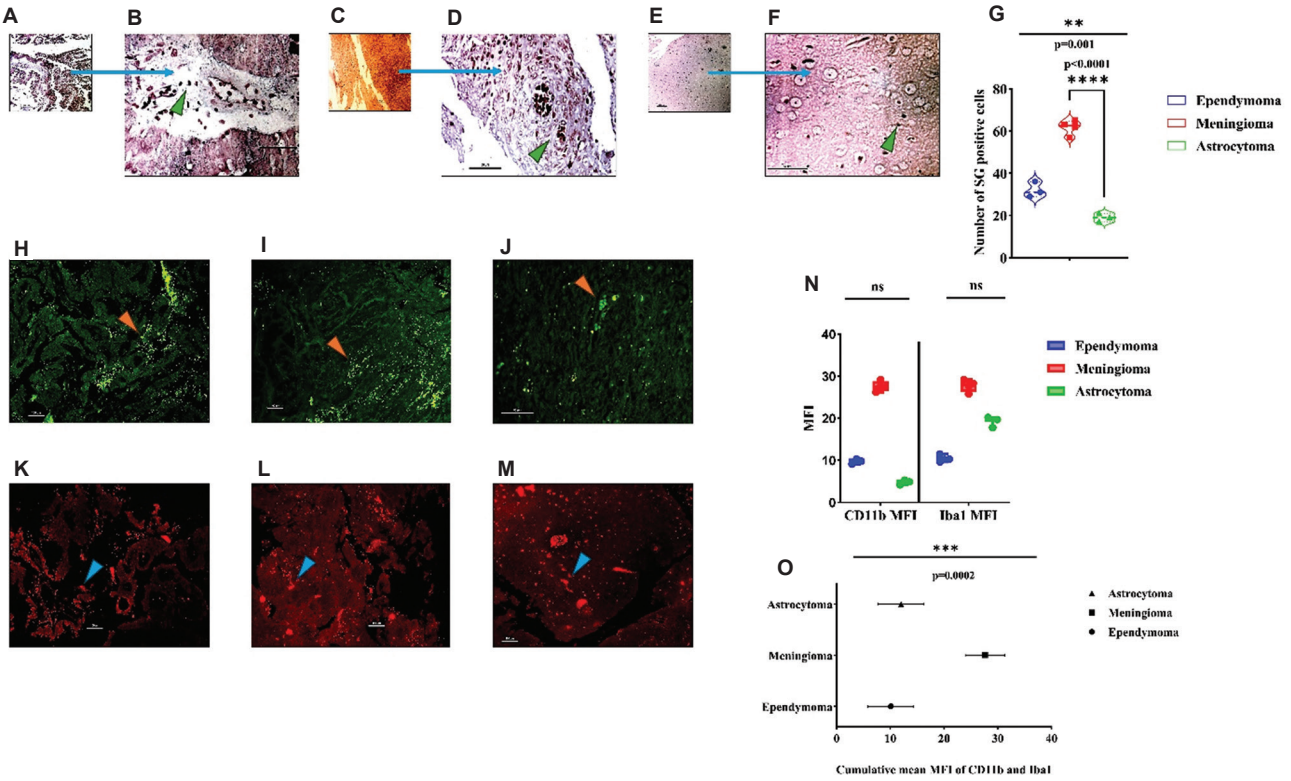

Figure 4. Evaluation of tumor-associated immune cells. Silver-gold (SG)-stained tissue sections at ×100 (scale bar: 100 µm) and ×400 (scale bar: 50 µm) magnification showing SG-positive immune cells (green arrows): (A and B) low-grade spinal myxopapillary ependymoma, (C and D) low-grade meningioma, (E and F) low-grade astrocytoma. (G) Violin plot comparing SG-positive cells density: ****$p \leq 0.0001$ (ependymoma vs. astrocytoma, *t*-test); **$p \leq 0.001$ (Kruskal–Wallis test); Immunofluorescence using CD11b-FITC (for detecting leukocytes, marked with orange arrows): (H) low-grade spinal myxopapillary ependymoma, (I) low-grade meningioma, (J) low-grade astrocytoma. Immunofluorescence using Iba1-PE (for detecting macrophage, marked with blue arrows): (K) ependymoma, (L) meningioma, (M) astrocytoma. (N) Clustered box plot for MFI values of CD11b-FITC and PE-Iba1: Not statistically significant (Kruskal–Wallis test). (O) Comparison of mean MFI (cumulative) of both CD11b and Iba1 across tumors analyzed through nested one-way ANOVA: ***$p \leq 0.001$.
Abbreviations: FITC: Fluorescein isothiocyanate; MFI: Mean fluorescence intensity.

pattern was consistent with the SG staining results and confirms a predominance of $CD11b^+$ myeloid cells in meningioma microenvironments.

In contrast, Iba1 immunofluorescence, which marks both resting and activated microglia, revealed a different pattern. Meningiomas exhibited the highest Iba1 MFI (27.72 ± 1.44; Figure 4L), followed by astrocytomas (19.23 ± 1.26; Figure 4M), and ependymomas (10.46 ± 0.96; Figure 4K). Although individual group comparisons for Iba1 did not reach statistical significance, these trends provided insights into the relative contributions from resident microglia and infiltrating macrophages (Figure 4N). Nested one-way ANOVA incorporating cumulative MFI values for CD11b and Iba1 revealed statistically significant differences in total mononuclear immune cell infiltration among all tumor subtypes (Figure 4O). This integrated analysis indicates that, despite variability in individual marker expression, each CNS tumor subtype exhibits a distinct immune microenvironment signature.

Astrocytomas exhibited a pronounced Iba1-predominant profile (Iba1:CD11b = 4:1), indicating preferential activation of resident microglial populations rather than recruitment of peripheral macrophages. This pattern aligns with the relative preservation of BBB in lower-grade astrocytic tumors, which limits peripheral immune cell infiltration while favoring localized microglial activation. These findings suggest that therapeutic strategies targeting microglial function, such as colony-stimulating factor 1 receptor (CSF1R) inhibitors or microglial repolarization agents, may be particularly effective in preventing tumor progression in astrocytomas. In addition, our observation of an inverse correlation between immune cell density and tumor aggressiveness challenges the conventional association between inflammation and malignancy in CNS tumors. The high immune cell infiltration in typically benign meningiomas, compared to the sparse immune presence in more aggressive astrocytomas, suggests that immune cell abundance may be a defining component of the CNS tumor microenvironment rather than a mere consequence of malignancy.

3.5. DNMT1 expression and epigenetic regulation patterns

Immunohistochemical analysis of DNMT1 expression in fixed tumor sections revealed distinct epigenetic patterns across CNS tumor subtypes. DNMT1-positive cells, identified by dark brown nuclear staining, demonstrated minimal expression in ependymomas (Figure 5A), a focal patchy distribution in meningiomas (Figure 5B), and markedly elevated expression in astrocytomas (Figure 5C). These findings suggest that differential epigenetic regulatory mechanisms may be operative across these tumor types.

The observed gradient of DNMT1 expression (ependymoma < meningioma < astrocytoma) implies that epigenetic dysregulation may serve as a key driver distinguishing indolent from more aggressive CNS tumors. This finding supports the notion that epigenetic alterations contribute significantly to malignant transformation. The elevated DNMT1 expression observed in astrocytomas identifies this tumor type as a potential candidate for methyltransferase inhibitor therapy, which could reverse the epigenetic silencing of tumor suppressor genes and potentially prevent progression to higher-grade malignancy.

4. Discussion

Comprehensive molecular characterization of low-grade CNS neoplasms represents a significant gap in the present neuro-oncological research, particularly when compared to their high-grade counterparts – particularly within the glioma spectrum.[1,18] This disparity may partly result from the often-subtle clinical manifestation of low-grade CNS tumors, resulting in delayed diagnosis or underreporting. However, such tumors can occasionally exhibit unexpected complications and poor prognostic outcomes.[19-21]

To address this gap, we conducted a study on selected low-grade primary CNS tumors, including grade I meningioma and ependymoma, and grade II diffused astrocytoma (noting that grade I astrocytomas are extremely

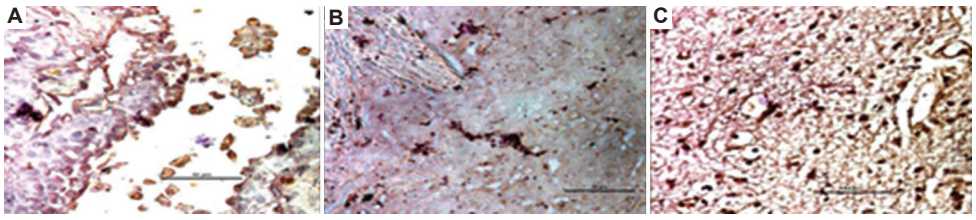

Figure 5. Epigenetic marker analysis. DNMT1 immunochemical imaging (×400, scale bar: 50 μm) showing methylation (brown patchy areas): (A) low-grade spinal myxopapillary ependymoma, (B) low-grade meningioma, and (C) low-grade astrocytoma.
Abbreviation: DNMT1: DNA methyltransferase 1.

rare and typically undiagnosed). Despite the limited sample size, our investigation revealed distinct patterns of cellular organization, proliferative potential, and tissue architecture. These features were closely associated with biological behavior and carry significant prognostic implications. Our findings highlight the critical need for enhanced molecular stratification strategies for low-grade CNS tumors. Such approaches could improve prognostic accuracy and guide therapeutic decisions. This preliminary investigation suggests an emerging pattern that may support prognostic assessment in low-grade CNS tumors.

Immunohistochemical and flow cytometric analyses revealed that neoplastic proliferation in WHO grade II diffuse astrocytomas – as quantified by GFAP immunoreactivity and Ki-67 index – demonstrated strong correlations with tumor cell proliferative activity and patient median overall survival.[22] Complementary demographic analyses conducted in South Indian populations corroborate these findings, demonstrating statistically significant associations between tumor proliferative capacity and clinical outcomes.[23] Although myxopapillary ependymomas comprise approximately 15% of all intramedullary spinal cord neoplasms and are traditionally classified as benign lesions with low Ki-67 indices, our molecular profiling paradoxically revealed elevated MMP-2 expression at both the cellular and tissue-architectural levels. This observation indicates an inverse correlation between proliferation and invasive potential, revealing a critical paradigm in CNS tumor biology. MMPs orchestrate extracellular matrix degradation, facilitate basement membrane disruption, and promote tumor cell invasion and potential metastasis. Previous investigations have documented significant correlations between elevated MMP-2 and MMP-14 expression levels across WHO grade I–III ependymomas and enhanced invasive behavior, which in turn correlate with poorer patient survival outcomes.[24]

Our comparative analysis of VEGFR2 expression, reflecting neoangiogenic activity, revealed heterogeneous patterns in myxopapillary ependymomas. These patterns suggest the presence of focal angiogenic switching in areas of gross total resection, despite the typically low proliferative indices observed. The angiogenic switch is governed by complex regulatory networks involving growth factor signaling pathways (e.g., epidermal growth factor, platelet-derived growth factor, and transforming growth factor) and tissue inhibitors of metalloproteinases modulation, which are influenced by tumor cells, stromal fibroblasts, infiltrating macrophages, and other immune cells. These elements collectively regulate MMP expression and VEGFR2-mediated signaling cascades.[25-27]

Taken together, our findings support a proliferation–invasion dichotomy with associated angiogenic implications among low-grade CNS tumors. Based on the molecular profiles observed, we propose that combination therapy targeting both MMP activity and neo-vasculogenesis may enhance treatment efficacy in low-grade spinal ependymoma. Similarly, dual inhibition of cell proliferation and neo-vasculogenesis may offer therapeutic benefits in low-grade astrocytic tumors. These approaches hold promise for preventing malignant progression while minimizing off-target cytotoxic effects.

Our previous investigations demonstrated a progressive accumulation of both brain-resident microglia and infiltrating macrophages across the malignancy spectrum from WHO grade II to grade IV astrocytomas. These myeloid cell populations play key roles in orchestrating extracellular matrix remodeling, which correlates directly with patient morbidity indices.[28] In the present study, quantitative analysis revealed the highest density of SG-stained, electron-dense microglia and macrophages in meningioma specimens, compared to astrocytomas and ependymomas. These findings were further corroborated through immunophenotyping using CD11b and Iba1 markers.

Previous reports have shown that the extradural location and arachnoid-derived origin of meningiomas – outside the constraints of the BBB – facilitate immune cell infiltration. In particular, meningiomas overexpress monocyte chemoattractant protein-1 (MCP-1), leading to the accumulation of tumor-associated macrophages of monocytic lineage and $CD8^+$ tumor-infiltrating lymphocytes. These immune cell populations are frequently associated with peri-tumoral edema, reflecting the complex interplay between tumor-secreted chemokines and vascular permeability factors. Conversely, the relatively sparse $CD11b^+$ cell populations observed in low-grade astrocytomas are consistent with the preserved integrity of the BBB. Tight junction proteins, such as claudin-5, occludin, and zonula occludens-1 help maintain BBB selectivity, thereby restricting the trans-endothelial migration of circulating monocytes and other peripheral immune effector cells at early stages of tumor development.[29,30] This barrier function, coupled with the typically low expression of MCP-1, limits peripheral monocyte recruitment. Instead, these tumors demonstrate predominant activation of brain-resident $Iba1^+$ microglia, which contribute to tumor progression through the evolving tumor–immune synapse.[31,32]

The differential abundance and spatial organization of resident microglia versus infiltrating macrophages within

Table 1. Comparative profiles of low-grade ependymoma, meningioma, and astrocytoma

Experimental parameters	Defining characteristics	WHO grade I myxopapillary ependymoma	WHO grade I fibrous meningioma	WHO grade II diffuse astrocytoma
Site of occurrence	Sub-regional location (as seen in MRI)	Extradural, spinal, involving the spinal canal extending from L1 – L5	Extracranial, midline basifrontal region	Intracranial, left temporo-parietal region
Magnetic resonance imaging (MRI)	T1	Hypointense	Iso to hypointense	Hypointense
	T2	Overall iso- to hyperintense	Iso to hyperintense	Markedly hyperintense
	Midline shift	Mild to negligible	Mild	Vividly observed
	Mass effect	Mild to negligible	Mild	Vividly observed
Magnetic resonance spectroscopy	Choline peak	High	High	High
	NAA peak	Low	Very low	Low
Histopathology under bright field microscopy	Hematoxylin and eosin staining (observed both in×10 [lower] and×40 [higher] magnification)	Lobulated islands, hyalinized fibrovascular core, perivascular pseudo-rosettes, lobulated blood islands, dystrophic micro-calcification	"Whorling" intercrossing fascicles, vascular sprouting, dystrophic micro-calcification	Fibrillary astrocytic processes, pleomorphic nucleus, conspicuous neovascularization, dystrophic micro-calcification
Astrocytic glial origin and proliferation	IF with GFAP-Alexa Fluor 488 to measure expressional intensity	Moderate	Least	Maximum
Gross proliferation	Proliferative index with IHC with Ki-67-HRP+hematoxylin counterstaining	Minimum (index value 0.62±0.09 SD)	Intermediate (index value1.34±0.36 SD)	Maximum (index value 2.1±0.16 SD)
	Tissue cell cycle analysis with PI	Total percentage of S+G2/M is minimum (8.63±0.51% SD)	Total percentage of S+G2/M is intermediate (12.60±0.70% SD)	Total percentage of S+G2/M is maximum (20.40±2.06% SD)
Angiogenic switching or neovascularization	IF with VEGFR2-TRITC to measure levels of angiogenic receptor expression (MFI)	Clustered/Patchy (30.1±2.38 SD)	Lowest (21.35±2.35 SD)	Highest (59.66±2.55 SD)
Metastatic nature or invasiveness	Cellular FC with MMP-2-PE	Highest	Intermediate	Lowest
	IF with MMP-2-FITC (MFI)	Regional intense expression (62.03±9.50 SD)	Low scattered expression (21.3±2.62 SD)	Diffused moderate expression (40.9±2.04 SD)
Association of mononuclear monocytic lineage Immune cells	S/G staining on fixed tissue (positive cells)	Moderate (32±3.60 SD)	Highest (62±3.40 SD)	Lowest (19±2 SD)
	IF with CD11b-FITC (MFI)	Moderate (9.73±0.60 SD)	Highest (27.57±1.23 SD)	Lowest (4.8±0.55 SD)
	IF with Iba1-PE (MFI)	Lowest (10.46±0.96 SD)	Highest (18.927.72±1.44 SD)	Moderate (19.23±1.26 SD)
Epigenetic alteration	Global methylation pattern detection by IHC with DNMT1-HRP+hematoxylin counterstaining	Scarce	Patchy and moderate	Diffuse but intense

Abbreviations: CD11b: Cluster of Differentiation 11b; DNMT1: DNA methyl transferase 1; FC: Flow cytometry; FITC: Fluorescein isothiocyanate; GFAP: Glial fibrillary acidic protein; HRP: Horse radish peroxidase; IHC: Immunohistochemistry; IF: Immunofluorescence; Ki-67: Kiel cell proliferating antigen protein 67; L1 – L5: Lumber region 1 – 5; MFI: Mean fluorescence index; MMP-2: Matrix metalloproteinase 2; NAA: N-acetylaspartate; PE: Phycoerythrin; PI: Propidium iodide; TRITC: Tetramethylrhodamine; SD: Standard deviation; S/G: Silver-gold staining; VEGFR2: Vascular endothelial growth factor receptor 2.

CNS tumors represent a fundamental pathophysiological determinant of tumor progression, therapeutic response, and clinical outcomes.[33] These immune microenvironmental characteristics are emerging as critical prognostic factors that merit further investigation.

Our findings support the development of precision therapeutic strategies that target microglia to prevent malignant progression in low-grade astrocytomas. CSF1R antagonists may effectively disrupt the CSF1/CSF1R signaling axis,[34] which is essential for microglial survival,

proliferation, and pro-tumorigenic M2 polarization. In addition, microglial repolarization strategies – employing CD40 agonists and/or STAT6 pathway inhibitors – may facilitate phenotypic switching from pro-tumorigenic M2 to anti-tumorigenic M1 activation states, thereby restraining transformation to higher-grade malignancies.[35,36]

In another aspect of the present study, DNMT1 expression across low-grade CNS tumor subtypes revealed the highest immunoreactivity in WHO grade II astrocytoma specimens, followed by intermediate levels in ependymomas. Non-glial meningiomas demonstrated moderate DNMT1 expression, suggesting distinct epigenetic regulatory mechanisms across tumor types. In our previous research, we observed a general trend of increasing epigenetic perturbation with higher glioma grades. However, a comprehensive analysis of epigenetic alterations in post-operative CNS tumor samples across different subtypes remains largely unexplored and may offer prognostic benefits.[37,38] The present study highlights the need for further rigorous investigations involving epigenomic profiling of grade-specific CNS neoplasms. Such studies could provide meaningful prognostic insights and facilitate the identification of novel therapeutic targets, including DNMT inhibitors, histone deacetylase (HDAC) inhibitors, O6-methylguanine-DNA methyltransferase (MGMT) inhibitors, and isocitrate dehydrogenase inhibitors. These agents may block malignant transformation through epigenetic reprogramming while reducing therapeutic resistance and minimizing off-target side effects.[39,40]

In summary, histopathological evaluation alone is insufficient for guiding anti-neoplastic treatment strategies. Prognostic success lies in understanding the functional potential of tumor cells and their microenvironmental interactions. Therefore, molecular characterizations at the cellular and tissue levels are indispensable for revealing hallmark tumor features, including proliferation, invasion, metastasis, neo-vasculogenic potency, and immune cell infiltration.[41]

Integrating cellular and molecular data with histopathological assessment is thus crucial for the rational design of effective anti-cancer treatment regimens. These findings underscore the importance of molecular and genetic tumor characterization, as emphasized in several recent studies.[10,42,43] Moreover, they highlight the need to examine inter- and intra-tumoral cellular organization within the CNS microenvironment – a highly influential factor influencing tumor progression and dissemination, even in low-grade lesions. To improve outcomes for patients with CNS tumors, including prolonged survival and enhanced quality of life, such diagnostic advancements must be incorporated at the early stages of clinical decision-making.

5. Conclusion

The study of low-grade CNS tumor samples from a hospital-based population revealed a non-linear and heterogeneous biological landscape (Table 1). The pathophysiological dynamics observed in WHO grade II diffuse astrocytomas and myxopapillary ependymomas – particularly the inverse correlations between proliferative capacity, invasive potential, and neoangiogenic activity – highlight the necessity of multimodal therapeutic approaches. These findings suggest that targeting interdependent oncogenic pathways simultaneously may be more effective than conventional single-agent strategies. For low-grade ependymomas, the strategic combination of MMP inhibitors with anti-angiogenic agents could synergistically disrupt the invasion–angiogenesis axis while minimizing the cytotoxic effects associated with anti-proliferative therapies. In contrast, patients with low-grade astrocytomas may benefit from the use of anti-proliferative agents, such as temozolomide in combination with therapies tailored to their unique molecular characteristics. These could include CSF1/CSF1R pathway antagonists or microglial repolarization agents targeting Iba1$^+$ microglial activity, anti-angiogenic therapies, and/or epigenetic reprogramming agents, such as DNMT inhibitors, MGMT inhibitors, and HDAC inhibitors. In low-grade meningiomas, where CD11b$^+$ macrophage infiltration is facilitated by their extradural location and absence of BBB constraints, immunotherapeutic interventions may hold particular promise, such as mTOR inhibitors (e.g., everolimus), CDK4/6 inhibitors, anti-invasive agents, and/or epigenetic modifiers depending on the minute biological properties of the tumor and physiological tolerance of the patients. Overall, this preliminary investigation suggests that several key hallmarks of cancer – proliferation, invasion, angiogenesis, and immune cell infiltration – may manifest distinctly even at early tumor grades, depending on CNS tumor subtype. Recognizing and addressing these subtype-specific patterns is essential for advancing personalized therapeutic strategies and optimizing clinical outcomes in patients with low-grade brain tumors.

Acknowledgments

The authors acknowledge Prof. S.N. Ghosh at the Neurosurgery Unit, Bangur Institute of Neurosciences (BIN), Institute of Post Graduate Medical Education and Research (IPGME&R), Kolkata, for helping in the collection of post-operative tumor samples, and Prof. Uttara Chatterjee of Pathology Department of IPGME&R for identifying and grading tumor samples.

Funding

This work was supported by the Council of Scientific and Industrial Research (CSIR), Government of India, through Project No. 37(1587)/13/EMR-II, and was partially supported by the Indian Council of Medical Research (ICMR) under project grant No. 61/8/2011-BMS, awarded to Dr. Anirban Ghosh as principal investigator.

Conflict of interest

The authors declare they have no competing interests.

Author contributions

Conceptualization: Anirban Ghosh
Data curation: Krishnendu Ghosh
Formal analysis: Krishnendu Ghosh
Funding acquisition: Anirban Ghosh
Investigation: Krishnendu Ghosh, Anirban Ghosh
Methodology: Krishnendu Ghosh
Project administration: Anirban Ghosh
Resources: Pritha Bhattacharjee, Anirban Ghosh
Supervision: Pritha Bhattacharjee, Anirban Ghosh
Validation: Pritha Bhattacharjee, Anirban Ghosh, Krishnendu Ghosh
Writing – original draft: Krishnendu Ghosh
Writing – review & editing: All authors

Ethics approval and consent to participate

The present study involved collection of post-operative human tumor samples, which was approved by the Institutional Ethical Committee (IEC) at the Institute of Post Graduate Medical Education and Research (IPGME&R), Kolkata, West Bengal, India (Human Ethical Clearance Memo No: Inst/IEC/553 dated January 15, 2014). The specimen collection was performed together with our collaborating neurosurgeon and clinical pathologist mentioned in the Acknowledgments section. Informed consent was obtained from the human subjects (patients' next keen) abiding by the World Medical Association- Declaration of Helsinki, 64th general assembly, Brazil, 2013.

Consent for publication

Informed consent was obtained from the human subjects (patients' next keen) to publish their data.

Availability of data

All the materials are owned by the authors and will be available from the corresponding authors upon reasonable request.

References

1. Dasgupta A, Gupta T, Jalali R. Indian data on central nervous tumors: A summary of published work. *South Asian J Cancer*. 2016;5(3):147-153.

   doi: 10.4103/2278-330X.187589

2. Ghosh A, Sarkar S, Begum Z, *et al*. The first cross sectional survey on intracranial malignancy in Kolkata, India: Reflection of the State of the art in Southern West Bengal. *Asian Pacific J Cancer Prev*. 2004;5(3):259.

3. Jalali R, Datta D. Prospective analysis of incidence of central nervous tumors presenting in a tertiary cancer hospital from India. *J Neurooncol*. 2008;87(1):111-114.

   doi: 10.1007/S11060-007-9487-Z

4. Paul M, Goswami S, Goutham Raj C, Bora G. Clinico-epidemiological profile of primary brain tumours in North-Eastern region of India: A retrospective single institution study. *Asian Pacific J Cancer Care*. 2023;8(2):333-336.

   doi: 10.31557/apjcc.2023.8.2.333-336

5. Yeole BB. Trends in the brain cancer incidence in India. *Asian Pac J Cancer Prev*. 2008;9(2):267-270.

6. Miller KD, Ostrom QT, Kruchko C, *et al*. Brain and other central nervous system tumor statistics, 2021. *CA A Cancer J Clin*. 2021;71(5):381-406.

   doi: 10.3322/CAAC.21693

7. Gao H, Jiang X. Progress on the diagnosis and evaluation of brain tumors. *Cancer Imaging*. 2013;13(4):466-481.

   doi: 10.1102/1470-7330.2013.0039

8. Park SH, Won J, Kim SI, *et al*. Molecular testing of brain tumor. *J Pathol Transl Med*. 2017;51(3):205-223.

   doi: 10.4132/jptm/2017.03.08

9. Louis DN, Perry A, Reifenberger G, *et al*. The 2016 World Health Organization classification of tumors of the central nervous system: A summary. *Acta Neuropathol*. 2016;131(6):803-820.

   doi: 10.1007/s00401-016-1545-1

10. Louis DN, Perry A, Wesseling P, *et al*. The 2021 WHO classification of tumors of the central nervous system: A summary. *Neuro Oncol*. 2021;23(8):1231-1251.

    doi: 10.1093/neuonc/noab106

11. Sincevičiūtė R, Vaitkienė P, Urbanavičiūtė R, Steponaitis G, Tamašauskas A, Skiriutė D. MMP2 is associated with glioma malignancy and patient outcome. *Int J Clin Exp Pathol*. 2018;11(6):3010-3018.

12. Seyedmirzaei H, Shobeiri P, Turgut M, Hanaei S, Rezaei N. VEGF levels in patients with glioma: A systematic review and meta-analysis. *Rev Neurosci*. 2020;32(2):191-202.

    doi: 10.1515/revneuro-2020-0062

13. Zheng Y, Graeber MB. Microglia and brain macrophages as drivers of glioma progression. *Int J Mol Sci*. 2022;23(24):15612.

doi: 10.3390/ijms232415612

14. Vidyarthi A, Agnihotri T, Khan N, *et al*. Predominance of M2 macrophages in gliomas leads to the suppression of local and systemic immunity. *Cancer Immunol Immunother*. 2019;68(12):1995-2004.

doi: 10.1007/s00262-019-02423-8

15. Rajendran G, Shanmuganandam K, Bendre A, Muzumdar D, Goel A, Shiras A. Epigenetic regulation of DNA methyltransferases: DNMT1 and DNMT3B in gliomas. *J Neurooncol*. 2011;104(2):483-494.

doi: 10.1007/s11060-010-0520-2

16. Zhao Y, Gan L, Ren L, Lin Y, Ma C, Lin X. Factors influencing the blood-brain barrier permeability. *Brain Res*. 2022;1788:147937.

doi: 10.1016/j.brainres.2022.147937

17. Alanen KA, Joensuu H, Klemi PJ. DNA ploidy and cell-cycle analysis in pancreatic and ampullary carcinoma: Flow cytometric study of formalin-fixed paraffin-embedded tissue. *Virchows Arch A Pathol Anat Histopathol*. 1991;419(3):255-256.

doi: 10.1007/BF01626357

18. Bready D, Placantonakis DG. Molecular pathogenesis of low-grade glioma. *Neurosurg Clin N Am*. 2019;30(1):17-25.

doi: 10.1016/j.nec.2018.08.011

19. Yrysov K, Arstanbekov N, Mamytov M, Akmataliev A, Turganbaev B, Vityala Y. Postoperative complications in patients with intracranial meningiomas who underwent surgery. *Biomedicine*. 2023;43(3):34-40.

doi: 10.51248/.v43i3.2886

20. Chang JH, Chang JW, Choi JY, Park YG, Chung SS. Complications after gamma knife radiosurgery for benign meningiomas. *J Neurol Neurosurg Psychiatry*. 2003;74(2):226-230.

doi: 10.1136/jnnp.74.2.226

21. Bertrand KC, Klimo P. Recent advancements in ependymoma: Challenges and therapeutic opportunities. *Pediatr Neurosurg*. 2023;58(5):307-312.

doi: 10.1159/000530868

22. Thotakura M, Tirumalasetti N, Krishna R. Role of Ki-67 labeling index as an adjunct to the histopathological diagnosis and grading of astrocytomas. *J Cancer Res Ther*. 2014;10(3):641-645.

doi: 10.4103/0973-1482.139154

23. Shivaprasad NV, Satish S, Ravishankar S, Vimalambike MG. Ki-67 immunostaining in astrocytomas: Association with histopathological grade - a South Indian study. *J Neurosci Rural Pract*. 2016;7(4):510-514.

doi: 10.4103/0976-3147.188626

24. Akyurek S, Chang EL, Yu TK, *et al*. Spinal myxopapillary ependymoma outcomes in patients treated with surgery and radiotherapy at M.D. Anderson cancer center. *J Neurooncol*. 2006;80(2):177-183.

doi: 10.1007/s11060-006-9169-2.

25. Snuderl M, Chi SN, De Santis SM, *et al*. Prognostic value of tumor microinvasion and metalloproteinases expression in intracranial pediatric ependymomas. *J Neuropathol Exp Neurol*. 2008;67(9):911-920.

doi: 10.1097/NEN.0b013e318184f413

26. Chen X, Li C, Che X, Chen H, Liu Z. Spinal myxopapillary ependymomas: A retrospective clinical and immunohistochemical study. *Acta Neurochir (Wien)*. 2016;158(1):101-107.

doi: 10.1007/s00701-015-2637-8

27. Ghosh K, Ghosh S, Chatterjee U, Chaudhuri S, Anirban A. Microglial contribution to glioma progression: An immunohistochemical study in Eastern India. *Asian Pac J Cancer Prev*. 2016;17(6):2767-2773.

28. Sato K, Kuratsu J, Takeshima H, Yoshimura T, Ushio Y. Expression of monocyte chemoattractant protein-1 in meningioma. *J Neurosurg*. 1995;82(5):874-878.

doi: 10.3171/jns.1995.82.5.0874

29. Lochhead JJ, Yang J, Ronaldson PT, Davis TP. Structure, function, and regulation of the blood-brain barrier tight junction in central nervous system disorders. *Front Physiol*. 2020;11:914.

doi: 10.3389/fphys.2020.00914

30. Yan D, Kowal J, Akkari L, *et al*. Inhibition of colony stimulating factor-1 receptor abrogates microenvironment-mediated therapeutic resistance in gliomas. *Oncogene*. 2017;36(43):6049-6058.

doi: 10.1038/onc.2017.261

31. Kvisten M, Mikkelsen VE, Stensjøen AL, Solheim O, Van Der Want J, Torp SH. Microglia and macrophages in human glioblastomas: A morphological and immunohistochemical study. *Mol Clin Oncol*. 2019;11(1):31-36.

doi: 10.3892/mco.2019.1856

32. Gutmann DH, Kettenmann H. Microglia/brain macrophages as central drivers of brain tumor pathobiology. *Neuron*. 2019;104(3):442-449.

doi: 10.1016/j.neuron.2019.08.028

33. Dubuc AM, Mack S, Unterberger A, Northcott PA, Taylor MD. The epigenetics of brain tumors. *Methods Mol Biol*. 2012;863:139-153.

doi: 10.1007/978-1-61779-612-8_8

34. Van Hooren L, Vaccaro A, Ramachandran M, *et al*. Agonistic CD40 therapy induces tertiary lymphoid structures but impairs responses to checkpoint blockade in glioma. *Nat Commun*. 2021;12(1):4127.

doi: 10.1038/s41467-021-24347-7

35. Tang F, Wang Y, Zeng Y, Xiao A, Tong A, Xu J. Tumor-associated macrophage-related strategies for glioma immunotherapy. *NPJ Precis Oncol*. 2023;7(1):78.

doi: 10.1038/s41698-023-00431-7

36. Skouras P, Markouli M, Papadatou I, Piperi C. Targeting epigenetic mechanisms of resistance to chemotherapy in gliomas. *Criti Rev Oncol Hematol.* 2024;104:104532.

doi: 10.1016/j.critrevonc.2024.104532

37. Ghosh K, Ghosh S, Chatterjee U, Bhattacharjee P, Ghosh A. Dichotomy in growth and invasion from low- to high-grade glioma cellular variants. *Cell Mol Neurobiol*. 2022;42(7):2219-2234.

doi: 10.1007/s10571-021-01096-1

38. Hanahan D, Weinberg RA. Hallmarks of cancer: The next generation. *Cell*. 2011;144(5):646-674.

doi: 10.1016/j.cell.2011.02.013

39. McClellan BL, Haase S, Nunez FJ, *et al*. Impact of epigenetic reprogramming on antitumor immune responses in glioma. *J Clin Invest*. 2023;133(2):e163450.

doi: 10.1172/JCI163450

40. Liu Y, Ali H, Khan F, Pang L, Chen P. Epigenetic regulation of tumor-immune symbiosis in glioma. *Trends Mol Med*. 2024;30(5):429-442.

doi: 10.1016/j.molmed.2024.02.004

41. Wang H, Diaz AK, Shaw TI, *et al*. Deep multiomics profiling of brain tumors identifies signaling networks downstream of cancer driver genes. *Nat Commun*. 2019;10(1):3718.

doi: 10.1038/s41467-019-11661-4

42. Ghosh A, Chaudhuri S. Tissue-free non-invasive diagnostic methodology for brain tumour: Present scenario and future direction. *Biomedicine*. 2019;44(1):39-45.

doi: 10.51248/.v44i1.4045

43. Heiden T, Castaños-Vélez E, Andersson LC, Biberfeld, P. Combined analysis of DNA ploidy, proliferation, and apoptosis in paraffin-embedded cell material by flow cytometry. *Lab Invest*. 2019;80(8):1207-1213.

doi: 10.1038/labinvest.3780128